ADVANCED FUNCTIONAL MATERIALS
www.afm-journal.de

High-Concentration Aqueous Dispersions of MoS_2

Yagang Yao, Lorenzo Tolentino, Zhongzheng Yang, Xiaojuan Song, Wen Zhang, Yongsheng Chen, and Ching-ping Wong**

Molybdenum disulfide (MoS_2) nanosheets have been attracting increasing research interests due to their unique material properties. However, the lack of a reliable large-scale production method impedes their practical applications. Here a facile, efficient, and scalable method for the fabrication of high-concentration aqueous dispersion of MoS_2 nanosheets using combined grinding and sonication is reported. The 26.7 ± 0.7 mg/mL concentration achieved is the highest concentration in an aqueous solution reported up to now. Grinding generates pure shear forces to detach the MoS_2 layers from the bulk materials. Subsequent sonication further breaks larger crystallites into smaller crystallites, which promotes the dispersion of MoS_2 nanosheets in ethanol/water solutions. The exfoliation process establishes a new paradigm in the top-down fabrication of 2D nanosheets in aqueous solution. In the meantime, MoS_2-based sensing film produced using this approach has successfully demonstrated the feasibility of a low-cost and efficient NH_3 gas sensor using inkjet printing as a viable method.

Dr. Y. G. Yao, L. Tolentino, Dr. Z. Z. Yang, Prof. C. P. Wong
School of Materials Science and Engineering
Georgia Institute of Technology
Atlanta, GA 30332, USA
E-mail: ygyao1511@gmail.com; cp.wong@mse.gatech.edu
Dr. Y. G. Yao
Suzhou Institute of Nanotech and Nanobionics
Chinese Academy of Science
Suzhou 215123, P. R. China
Dr. Z. Z. Yang
School of Civil Engineering and Communication
North China University of Water Resources and Electric Power
Zhengzhou, Henan 450011, P. R. China
Dr. X. J. Song
Electro-Optical System Lab
Georgia Technology Research Institute
Georgia Institute of Technology
Atlanta, GA 30332, USA
Dr. W. Zhang, Prof. Y. S. Chen
School of Civil and Environmental Engineering
Georgia Institute of Technology
Atlanta, GA 30332, USA
Dr. W. Zhang
Department of Civil and Environmental Engineering
New Jersey Institute of Technology
Newark, NJ 07102, USA
Prof. C. P. Wong
Department of Electronic Engineering
Faculty of Engineering
The Chinese University of Hong Kong
ShaTin, Hong Kong

DOI: 10.1002/adfm.201201843

1. Introduction

Molybdenum disulfide (MoS_2) nanosheets, as one of the inorganic graphene analogues and a member of the transition metal dichalcogenides (TMDs), have recently received great attention due to their unusual and excellent properties correlated with its 2D ultrathin atomic layer structure.[1–30] Bulk MoS_2 is an n-type semiconductor with an indirect band gap of about 1.2 eV. When layered MoS_2 crystal is thinned to monolayer, it turns into a 1.8 eV direct band gap semiconductor.[7,22,30] This large band gap is a big advantage for monolayer MoS_2 over graphene because in its pristine form, graphene has zero band gap and band gaps up to 400 meV have to be introduced by unzipping carbon nanotubes (CNTs) into graphene nanoribbons or applying high transverse electric fields to bilayer graphene, resulting in significant mobility reduction, or loss of coherence, or small current on/off ratios in graphene field effect transistors (FETs).[31–38] Using a hafnium oxide (HfO_2) gate dielectric, monolayer MoS_2 FETs were demonstrated to be useful transistors, and an electron mobility of more than 200 $cm^2\ V^{-1}\ s^{-1}$ and current on/off ratios of up to 10^8 were achieved.[9] Zhang et al. fabricated a new phototransistor based on the mechanically exfoliated monolayer MoS_2 nanosheets. The monolayer MoS_2 phototransistor exhibits fast switching behavior with the photocurrent generation and annihilation finishing within ca. 50 ms, and good stability.[2] Importantly, the device shows a better photoresponsivity (7.5 mA/W) as compared with the graphene-based device (1 mA/W) which mainly arises from the rapid electron-hole recombination induced by the intrinsic property of zero band gap and fast carrier transfer of graphene.[31,32] Kis et al. demonstrate that monolayer MoS_2 has the capability of amplifying signals and performing basic logic operations in simple integrated circuits composed of two MoS_2 transistors.[3] They also proposed that MoS_2 has advantages over conventional silicon: it is thinner than state-of-the-art silicon films that are 2 nm thick and has a smaller dielectric constant (ε = 7) than silicon (ε = 11.9), indicating that using monolayer MoS_2 could reduce short channel effects and result in smaller and less power hungry transistors than those based on silicon technology. Strong photoluminescence emerges in ultrathin layers of MoS_2 while the photoluminescence is absent in bulk material, indicating an indirect to direct band gap transition when the thickness is decreased from bulk to monolayer.[13] Cho et al. also found out that MoS_2 nanosheets, consisting of disordered graphene-like layers, are good high rate lithium battery anode materials.[11]

However, large-scale preparation of MoS_2 nanosheets have to be fulfilled before MoS_2 nanosheets can actually become a mainstream electronic material for the semiconductor industry. A major breakthrough was made by the exfoliation of layered MoS_2 materials in various organic solvents via sonication to generate mono- or multilayer structures.[12] The concentration of the resulting MoS_2, about 0.3 mg/mL, is still low for large-scale applications. In addition, the solvents used are expensive and toxic, requiring special care during handling, and have high boiling points, which makes it difficult to be removed. Later, an improved exfoliation method in an aqueous surfactant solution via high power tip sonication was reported. But the achieved concentration (approximately 0.25 mg/mL) is still not high enough.[8] Zhou et al. reported that a mixed-solvent, ethanol/water at an appropriate ratio, can be used to exfoliate MoS_2. Despite the low cost, the concentration of 0.018 mg/mL achieved is fairly low.[5] Recently, ≈40 mg/mL MoS_2 dispersion was successfully prepared in organic solvents by more than a hundred hours of sonication,[39] which, however, could damage MoS_2 nanosheets and affect its properties. Zhang et al. have demonstrated a controllable lithium intercalation process via incorporating the layered bulk materials, such as MoS_2, as the cathode in an electrochemical set-up.[6] The shortcoming of this method is the complicated electrochemical process, which may limit its applications. Thin layers of MoS_2 were also synthesized via a two-step thermolysis process or a two-step thermal evaporation-exfoliation method.[15,40] However, the high temperature process is unfavorable for applications in electronic and optical device fabrication industries. Hence, it is highly desirable to develop a new strategy to produce MoS_2 nanosheets on a large scale to promote their practical applications.

In this study, we have developed a less energy intensive shearing process for the direct exfoliation of bulk MoS_2 crystal into monolayer and few-layer MoS_2 nanosheets, namely combined *N*-methyl-2-pyrrolidone (NMP) assisted grinding and sonication (in mixed solvent, ethanol/water). We have tailored the time of grinding from 30 min to 3 h, and the combination of grinding and sonication to produce higher concentration of MoS_2 nanosheets in aqueous solutions than the reported values in literatures. Few-layer and monolayer MoS_2 are achieved in ethanol/water solutions, which are ready for large-scale electronic, optoelectronic, and photovoltaic applications. The exfoliation process establishes a new paradigm in the top-down fabrication of 2D nanosheets in aqueous solution, and we demonstrate that this approach is very useful in the construction low-cost, high-performance MoS_2 materials-based gas sensing devices, such as for NH_3 gas sensing at ambient environment. We also illustrate inkjet printing as a viable method for large-area fabrication of MoS_2 materials-based devices.

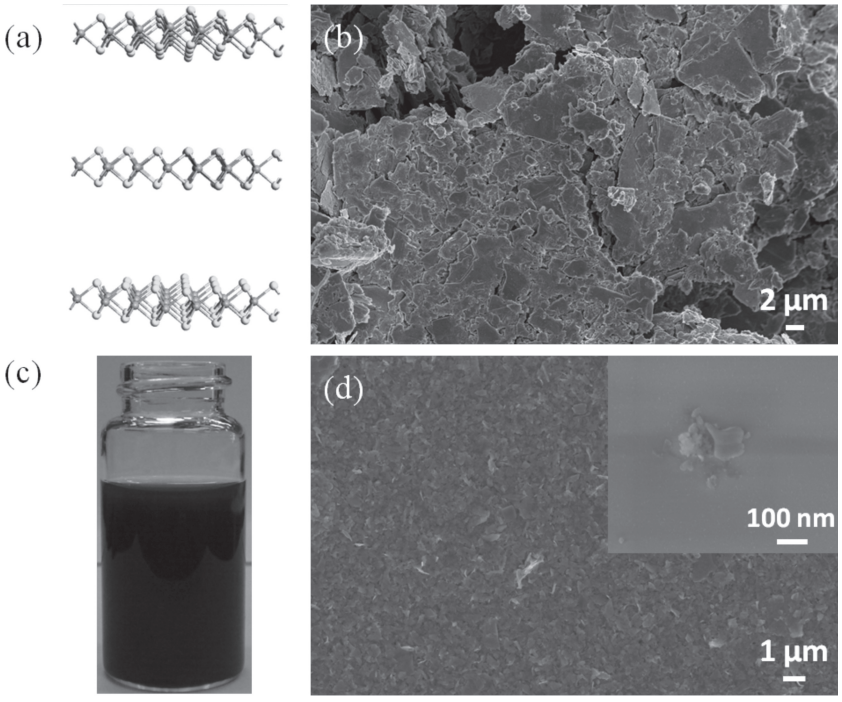

Figure 1. a) Schematic of bulk MoS_2 structure. Mo atoms are blue in color and S atoms yellow. b) SEM image of raw MoS_2 materials. c,d) Optical microscopy image (in ethanol/water solution) and SEM image of MoS_2 nanosheets by combined grinding (3 h) and sonication (2 h), respectively. Inset in (d) is a magnified SEM image of MoS_2 nanosheets deposited on a silicon substrate.

2. Results and Discussion

Bulk MoS_2 is depicted by layered crystal structures with 2D layers composed of strong S–Mo–S intralayer covalent bonding shown in **Figure 1**a. The bonding between layers is van der Waals in nature, showing very weak interlayer interaction. Here, we used a less energy intensive shearing process for exfoliating MoS_2, namely combined grinding and sonication. The grinding process is mild and relies on pure shear forces to detach the MoS_2 layers from the bulk materials. Thus, severe defect formation on the crystalline plane of graphene is avoided. NMP is used during the grinding, which acts as a stabilizing surfactant to avoid reassembling/restacking of the MoS_2 nanosheets during the grinding process. Other organic solvents such as dimethylformamide (DMF) and dimethylsulphoxide (DMSO) are also used during the grinding. After grinding, short time sonication is applied to further exfoliate MoS_2 in 45 vol% ethanol/water solution. It was demonstrated that 45 vol% ethanol/water solution gives high solubility to MoS_2 nanosheets based on the theory of Hansen solubility parameters (HSP).[5]

To demonstrate the exfoliating effect of the combined grinding and sonication, firstly we investigated the exfoliation of bulk MoS_2 by grinding for 3 h in NMP and then sonication in ethanol/water solution for 2 h. The starting MoS_2 powder has representative lateral particle sizes in the range of 0.5–10 μm as shown in Figure 1b. A typical photograph of MoS_2 suspension by 3 h grinding and 2 h sonication after centrifugation is shown in Figure 1c. The concentration of as-fabricated MoS_2 suspension was determined to be approximately 26.7 mg/mL, by

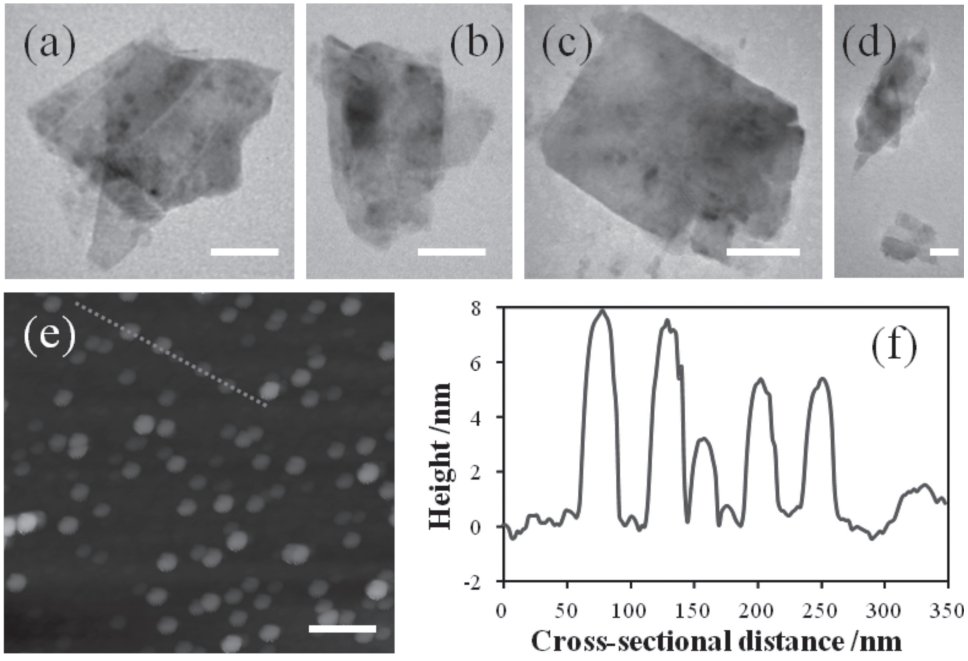

Figure 2. Typical TEM images (a–d; scale bar is 25 nm) and AFM (e; scale bar is 100 nm) of MoS_2 nanosheets exfoliated by combined grinding (3 h) and sonication (2 h). f) AFM height profile across the MoS_2 nanosheets in panel (e).

measuring the weight of MoS_2 nanosheets in 20 mL of supernatant from centrifugation. The dispersion was stable over the period of hundreds of hours. Zeta potential of the as-prepared MoS_2 aqueous dispersion was measured, which explained its excellent aqueous stability. The dispersed MoS_2 was negatively charged, with a zeta potential of –22.7 ± 1.3 mV. The high surface charge induced high electrostatic repulsion between MoS_2 nanosheets, which kept them stable in the aqueous dispersion. The film of MoS_2 nanosheets produced by vacuum filtration is shown in Figure 1d. In the scanning electron microscopy (SEM) image, the nanosheets show a certain transparency under SEM electron beam due to their small thickness. The SEM images in Figure 1b,d, and the inset in (d) clearly indicate that both the lateral sizes and the thicknesses of layered MoS_2 were reduced by combined grinding and sonication. Transmission electron microscopy (TEM) and atomic force microscopy (AFM) were also used to further analyze the structures of MoS_2 nanosheets directly from the as-fabricated dispersion, which contains large quantities of ultrathin 2D nanosheets (**Figure 2**). Examples of very thin sheets examined by TEM are shown in Figure 2a–d. Due to its ultrathin structure, the MoS_2 nanosheets turn slightly transparent to the electron beam. The lateral size of MoS_2 nanosheets is typically 20 to 70 nm. Electron diffraction patterns in Figure S1 (Supporting Information) reveal typical six-fold symmetry natural of MoS_2. Exfoliated MoS_2 nanosheets can be deposited on substrates by spin-coating. Figure 2e is an AFM image of MoS_2 nanosheets deposited on a silicon wafer. The nanosheets observed are tens of nanometers wide, in agreement with the TEM data. AFM imaging of individual nanosheets (Figure 2f) show that the thicknesses varied from 1.2 to 8.5 nm and sizes from 20 to 60 nm. Figure S2 (Supporting Information) is an additional AFM image at a higher magnification, which shows better contrast for the edge boundary, size, and morphology of MoS_2 nanosheets. The nanosheets consisted of MoS_2 as confirmed by Raman spectra (**Figure 3**) and UV-visible spectra (Figure 4d) In the UV-visible spectra, the diluted MoS_2 dispersion exhibited two peaks at 627 nm and 672 nm, which can be attributed to the characteristic A1 and B1 direct excitonic transitions of MoS_2 with the energy split from valence band spin-orbital coupling.[12] The optical absorbance increased with the increase of the concentration.

In Figure 3, the two Raman peaks correspond to the high energy mode A_{1g} mode and lower energy E_{2g} mode. A_{1g}

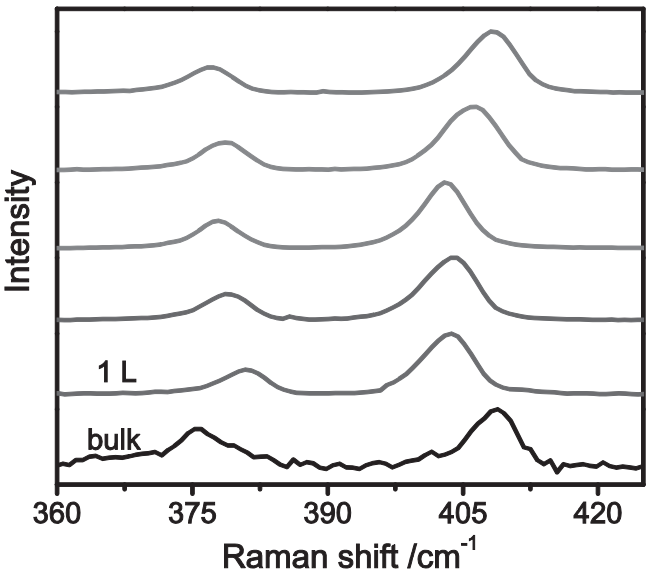

Figure 3. Typical Raman spectra of bulk MoS_2 and MoS_2 nanosheets exfoliated by combined grinding (3 h) and sonication (2 h). The spectra were normalized with the A_{1g} mode.

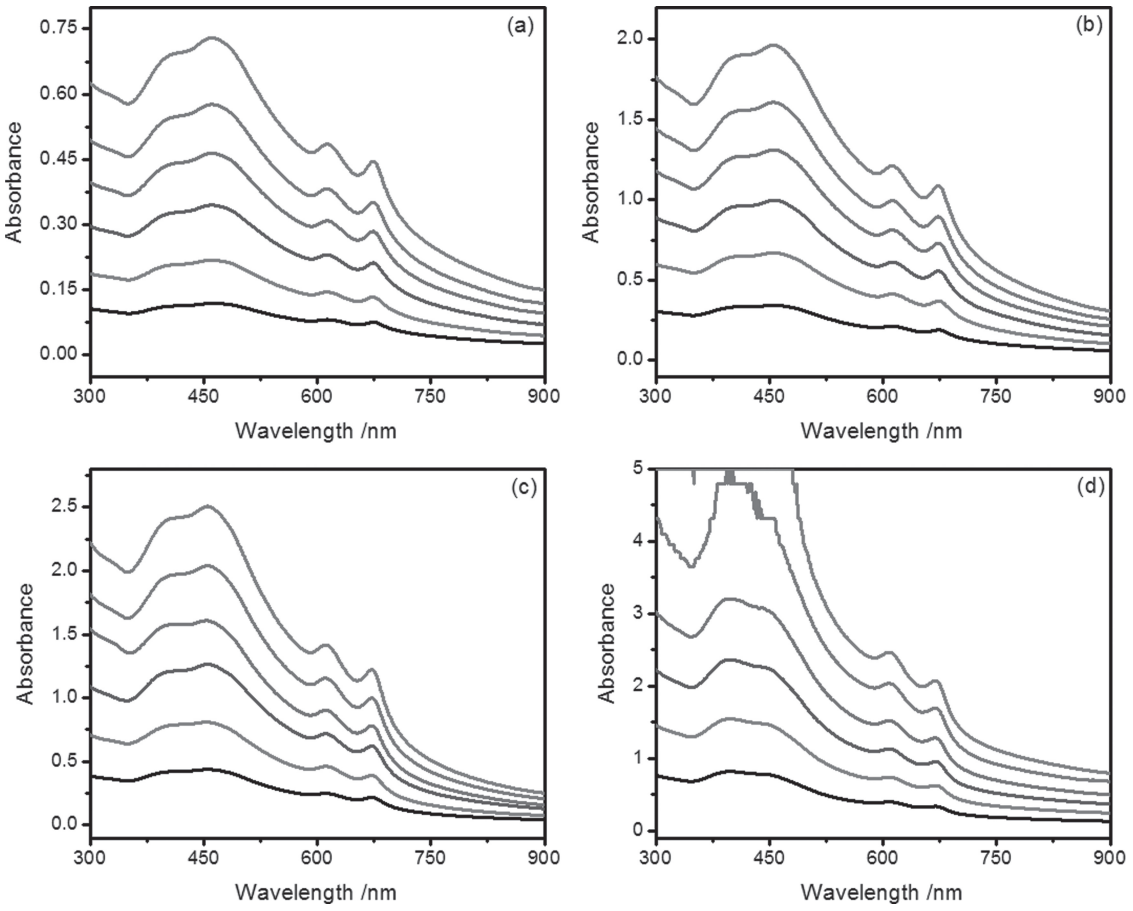

Figure 4. UV-visible absorption spectra of exfoliated MoS_2 nanosheets by combined grinding for 0.5 h (a), 1 h (b), 2 h (c), and 3 h (d) and sonication for 2 h. The concentration increases from the bottom spectrum to the top one. a) The concentrations are 1.3×10^{-3}, 2.2×10^{-3}, 3.7×10^{-3}, 4.9×10^{-3}, 5.2×10^{-3}, and 7.0×10^{-3} mg/mL, respectively. b) The concentrations are 2.7×10^{-3}, 5.5×10^{-3}, 8.2×10^{-3}, 10.9×10^{-3}, 13.6×10^{-3}, and 16.4×10^{-3} mg/mL, respectively. c) The concentrations are 3.5×10^{-3}, 7.1×10^{-3}, 10.6×10^{-3}, 14.1×10^{-3}, 17.6×10^{-3}, and 21.2×10^{-3} mg/mL, respectively. d) The concentrations are 3.7×10^{-3}, 7.6×10^{-3}, 11.2×10^{-3}, 14.9×10^{-3}, 18.7×10^{-3}, and 22.4×10^{-3} mg/mL, respectively.

mode and E_{2g} mode exhibit a well-defined thickness dependence, with the two modes shifting away from each other in frequency with increasing thickness, red shifts of E_{2g} mode and blue shifts of A_{1g} mode, which are consistent with the results in the literature.[41] The number of layers can almost be estimated according to the Raman data.[12,41,42] Single layer, double layer and few layer MoS_2 nanosheets were found in the sample. We can easily determine that red curve is from single layer MoS_2. The A_{1g} mode (red curve) is very well described by a single Lorentzian centered at 403.6 (red curve) cm^{-1} with a full width at half maximum (FWHM) of 6.1 cm^{-1}. The centre and width values are close to those observed for single layer MoS_2 sheets exfoliated mechanically, indicating the success of making single layer MoS_2 nanosheets.[12,41,42] The E_{2g} mode is centered at 381.0 cm^{-1} (red curve) with an FWHM of 5.2 cm^{-1}. This is significantly different from the published vales of 382–385 cm^{-1}.[41] In order to know why there is a shift for E_{2g} mode for the exfoliated MoS_2 nanosheets, firstly, we conducted energy-dispersive X-ray spectroscopy (EDXS) on bulk MoS_2 (Supporting Information Figure S3a) and MoS_2 nanosheets (Supporting Information Figure S3b) exfoliated by combined grinding (3 h) and sonication (2 h). Three elements (Mo, S and C) were detected. The C peak is largely ascribed to the conductive carbon tape underneath MoS_2 thin films. Therefore, we believe the E_{2g} shift is probably not due to the impurity or intercalation embedded into MoS_2 layers. Secondly, we did Raman on bulk MoS_2 material. A lower frequency of E_{2g} mode was observed at 375.4 cm^{-1}, compared to bulk MoS_2 material at 382 cm^{-1} in the literature.[41] The reason for this discrepancy remains unclear at present. We think the E_{2g} mode shift of bulk MoS_2 material is the main reason for the Raman shift for the exfoliated MoS_2 layers.

To verify the exfoliation effect caused by grinding, we have tailored the time of grinding from 0.5 h to 3 h with the same duration of sonication (2 h). Zeta potentials of the as-prepared dispersions after centrifugation are –29.4 ± 1.6,–26.5 ± 1.5, and–24.2 ± 1.3 mV for the samples by 0.5, 1, and 2 h grinding, respectively, indicating that they were negatively charged and stable in dispersion. **Figure 4** shows UV-visible absorption spectra of exfoliated MoS_2 nanosheets by combined grinding for 0.5 h (Figure 4a), 1 h (Figure 4b), 2 h (Figure 4c), and 3 h (Figure 4d) and sonication for 2 h. All the spectra exhibit two typical peaks of MoS_2 at 627 nm and 672 nm, indicating the existence of MoS_2 nanosheets. With increasing the concentration, the

Table 1. Concentration results of MoS_2 nanosheets in ethanol/water solutions by combined different durations (0.5, 1, 2, and 3 h) of grinding and 2 h of sonication.

Grinding time [h]	Concentrations measured by filtration [mg/mL]
0.5	6.8 ± 0.4
1	15.3 ± 0.6
2	23.6 ± 0.5
3	26.7 ± 0.7

optical absorbance increased. We calculated the concentrations *C* of the samples made by different durations of grinding and 2 h of sonication by measuring the weight of MoS_2 nanosheets in 20 mL of supernatant. **Table 1** shows concentration results of MoS_2 nanosheets in ethanol/water solutions. It is obvious that with the increase of grinding time, the concentration of MoS_2 nanosheets in ethanol/water solutions increase but not linearly. Grinding for 2 h resulted in a similar concentration with that for 3 h of grinding. Accordingly, the most efficient exfoliation should occur in the first 2 h of grinding. TEM was used to characterize the sizes of MoS_2 nanosheets by different durations of grinding. Shown in Supporting Information Figure S3 are TEM images of MoS_2 nanosheets exfoliated by combined different durations (0.5, 1, and 2 h) of grinding and 2 h of sonication. TEM results in Figure 2a–d and Supporting Information Figure S3 show that the sample from 0.5 h grinding seemed to be thicker than other samples, but we are not able to see the big difference in sizes from TEM images. Supporting Information Figure S4a shows the AFM image of MoS_2 nanosheets by 1 h of grinding spin-coated on a silicon wafer and the typical thicknesses was 3.5 to 17.4 nm and sizes ranged from 25 to 120 nm. Based on the AFM images in Figure 2e (3 h grinding) and Supporting Information Figure S4a (1 h), the MoS_2 nanosheets produced from different grinding times have quite different lateral and height distribution and the longer grinding time produces small sizes of nanosheets with narrower distribution. We also kept the same duration of grinding (0.5 h) and tailored the time of sonication to investigate the exfoliation effect caused by sonication. Supporting Information Figure S5 shows optical microscopy images of MoS_2 dispersions after centrifugation by 0.5 h of grinding and different durations of sonication. With increasing the sonication time, the concentration of MoS_2 nanosheets in ethanol/water solutions increased. The above results indicate that using combined grinding and sonication, high-concentration aqueous MoS_2 dispersions can be successfully obtained. These 2D nanosheets were further demonstrated for large-scale electronic, optoelectronic, and photovoltaic applications.

High-concentration aqueous dispersions of MoS_2 nanosheets discussed above, together with their large surface area and strong adsorbability, allow us to investigate their potential application as a gas sensor. NH_3 is a colorless, highly toxic gas with a special odor, is flammable between 16–25% by volume, and is very harmful to the human body as it has the potential to harm tissues, to affect the immune system, and to inhibit growth in cell lines, with 300 ppm IDLH (immediately dangerous to life or health). Therefore, the ammonia sensing system is extremely important to the environment, medical practice, and personnel safety as well as property protection.[43] Here, exfoliated MoS_2 nanosheets by combined 3 h of grinding and 2 h of sonication were used as chemresistor based gas sensors. We employed inkjet printing to deposit MoS_2 nanosheets onto pre-prepared microelectrode, which enabled us to monitor the resistance change when various ambient were used. The sensing performance of as-fabricated MoS_2-based devices was characterized under ambient conditions (i.e., atmospheric pressure and room temperature) against NH_3. As shown in **Figure 5**, such MoS_2-based gas sensors exhibited good sensitivity towards NH_3, which can detect several ppm of NH_3 gas. While these properties endow MoS_2 2D nanosheets with great promise as NH_3 gas sensor, further optimization is needed to reduce their recovery time.

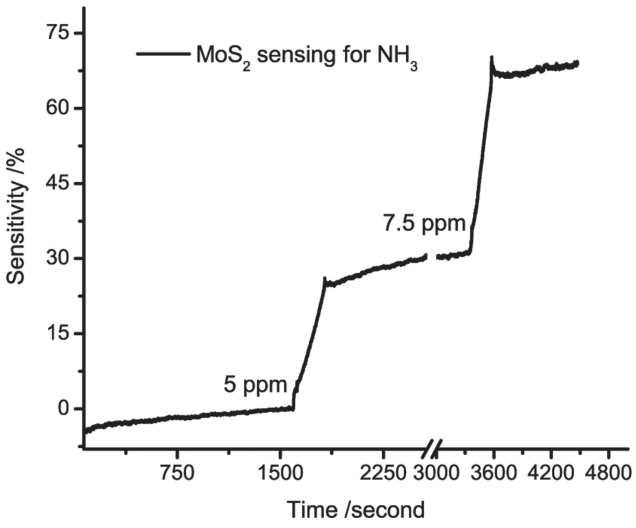

Figure 5. The sensitivity of MoS_2-based gas sensing devices toward NH_3.

3. Conclusions

In summary, we present a facile, scalable method to fabricate high-concentration aqueous dispersions of MoS_2 nanosheets using combined grinding and sonication. The as-fabricated dispersions consist of monolayer and few-layer 2D nanosheets and are relatively stable. MoS_2-based sensing film produced through this approach has been successfully applied in low-cost, high performance gas sensing device. We also demonstrate inkjet printing as a viable method for large-area fabrication of MoS_2 devices.

4. Experimental Section

Monolayer and Few-Layer MoS_2 Preparation and Characterizations: Layered MoS_2 materials (99.0% purity, 800 mg) with a grain size less than 10 μm were ground with NMP (0.4 mL) for different durations (0.5, 1, 2, and 3 h) in a mortar shown in Supporting Information Figure S6. Then the gel-like mixtures were put into a vacuum oven at 60 °C to evaporate the solvents. After that, the powder were dispersed in 45 vol%

ethanol/water mixture (20 mL) and sonicated for different durations (3, 10, 20, 30, 60 and 120 min) and then centrifugated at the speed of 6000 rpm for 30 min. The supernatant was collected, with which the MoS_2 samples were prepared for the study of their microstructure and optical properties. The suspension was diluted and dropped on lacy carbon-coated Cu grid for TEM observations, and on clean thermally oxidized Si wafer substrates (300 nm SiO_2) for Raman, SEM, EDXS, and AFM studies. TEM images were obtained using JEOL TEM 100CX. AFM images were acquired using the Agilent 5500 Molecular Imaging AFM. The morphologies of MoS_2 nanosheets were obtained using SEM (JEOL 1530 and 1550). Because of their weak contrast caused by very thin nanosheets, the vacuum filtrated films and 2D MoS_2 nanosheets deposited on SiO_2 substrates were covered by the conductive tape both on the bottom and top surfaces for SEM examination. Raman characterization was carried out using LabRAM ARAMIS, Horiba Jobin Yvon with a 532-nm-wavelength laser. UV-visible spectra were measured by UV-2450 (Shimadzu Co.). It is worth noting that the sediment on the bottom of the centrifugation tube could be re-dispersed in 45 vol% ethanol/water solution via sonication without the second-time grinding. Zeta potentials of MoS_2 nanosheets in 45 vol% ethanol/water solution made by different durations of combined grinding and sonication were collected with a Malvern Zetasizer.

Concentrations Measurement: To determine the concentrations of MoS_2 nanosheets in the supernatant from centrifugation, we measured the weight of MoS_2 nanosheets in the supernatant (20 mL). A precisely measured 20 mL of the dispersion was filtered under high vacuum onto a filter membrane of known mass. The resulting film was washed with large amount of hot water and ethanol and dried in a vacuum oven at 60 °C for 24 h. The mass of MoS_2 nanosheets in the filtered volume of stock dispersion was then determined using a microbalance.

Inkjet Printing of MoS_2 for Sensing: Glycerol was added to MoS_2-ethanol-water dispersion with a weight ratio of 1:3 (glycerol: MoS_2-ethanol-water) to meet the viscosity and surface tension requirements for inkjet printing. MicroFab jetlab II inkjet deposition system was used for inkjet printing of MoS_2 ink onto the SiO_2 substrate. The temperature of printer platen was set to 60 °C to assist in the evaporation of water and glycerol and the print head was set at 40 °C. The MoS_2 ink was printed via following procedures: First, 15 layers of MoS_2 were deposited with periodically cleaning the print head; then the MoS_2 on SiO_2 was baked at 80 °C in an oven to remove the solvent and any traces of glycerol.

Controlled Sensor Measurement: The controlled measurement system consisted of five major components: a gas generator, a nitrogen cylinder for gas-flow dilution, a NH_3 permeation tube, a closed-system sensor cell, and a data acquisition system. A 491MB gas generator and the NH_3 permeation tube, shown in Figure S7, from Kin-Tek Company (La Marque, TX) were used and the sensitivity measurements were performed under a chemical fume hood at room temperature. The NH_3 permeation tube had a calibrated emission rate under controlled temperature. Dry nitrogen was delivered from an ultrahigh purity (Grade 5) compressed nitrogen gas cylinder from Airgas. By controlling the NH_3 emission rate and the nitrogen flow rate, desired concentrations (in ppm range) of NH_3 were generated from the gas generator. Before each NH_3 exposure test, the NH_3 permeation tubes were installed in the gas generator and heated to a predetermined temperature for around 4 h in order to obtain a stabilized NH_3 concentration. The accuracy of gas concentration output is ±4% according to the calibration results from Kin-Tek. The sensor was installed inside a closed test cell. The concentrated NH_3 stream was delivered into the test cell via a Teflon tube. The printed MoS_2 film was placed near the gas inlet port, so that the NH_3 stream were allowed to interact with the sensor surface first. Resistance measurement of the sensor exposed to NH_3 vapor was performed using a data acquisition system (Keithley 2700).

Supporting Information

Supporting Information is available from the Wiley Online Library or from the author.

Acknowledgements

The authors would like to thank Dr. Tim Zhang and the Georgia Technology Research Institute.

Received: July 5, 2012
Revised: January 9, 2013
Published online: February 27, 2013

[1] Y. Yao, Z. Lin, Z. Li, X. Song, K.-S. Moon, C.-P. Wong, *J. Mater. Chem.* **2012**, *22*, 13494.
[2] Z. Yin, H. Li, H. Li, L. Jiang, Y. Shi, Y. Sun, G. Lu, Q. Zhang, X. Chen, H. Zhang, *ACS Nano* **2012**, *6*, 74.
[3] B. Radisavljevic, M. B. Whitwick, A. Kis, *ACS Nano* **2011**, *5*, 9934.
[4] H. Li, Z. Yin, Q. He, H. Li, X. Huang, G. Lu, D. W. H. Fam, A. I. Y. Tok, Q. Zhang, H. Zhang, *Small* **2012**, *8*, 63.
[5] K.-G. Zhou, N.-N. Mao, H.-X. Wang, Y. Peng, H.-L. Zhang, *Angew. Chem. Int. Ed.* **2011**, *50*, 10839.
[6] Z. Zeng, Z. Yin, X. Huang, H. Li, Q. He, G. Lu, F. Boey, H. Zhang, *Angew. Chem. Int. Ed.* **2011**, *50*, 11093.
[7] Y. Yoon, K. Ganapathi, S. Salahuddin, *Nano Lett.* **2011**, *11*, 3768.
[8] R. J. Smith, P. J. King, M. Lotya, C. Wirtz, U. Khan, S. De, A. O'Neill, G. S. Duesberg, J. C. Grunlan, G. Moriarty, J. Chen, J. Wang, A. I. Minett, V. Nicolosi, J. N. Coleman, *Adv. Mater.* **2011**, *23*, 3944.
[9] B. Radisavljevic, A. Radenovic, J. Brivio, V. Giacometti, A. Kis, *Nat. Nanotechnol.* **2011**, *6*, 147 .
[10] D. Kim, D. Sun, W. Lu, Z. Cheng, Y. Zhu, D. Le, T. S. Rahman, L. Bartels, *Langmuir* **2011**, *27*, 11650.
[11] H. Hwang, H. Kim, J. Cho, *Nano Lett.* **2011**, *11*, 4826.
[12] J. N. Coleman, M. Lotya, A. O'Neill, S. D. Bergin, P. J. King, U. Khan, K. Young, A. Gaucher, S. De, R. J. Smith, I. V. Shvets, S. K. Arora, G. Stanton, H.-Y. Kim, K. Lee, G. T. Kim, G. S. Duesberg, T. Hallam, J. J. Boland, J. J. Wang, J. F. Donegan, J. C. Grunlan, G. Moriarty, A. Shmeliov, R. J. Nicholls, J. M. Perkins, E. M. Grieveson, K. Theuwissen, D. W. McComb, P. D. Nellist, V. Nicolosi, *Science* **2011**, *331*, 568.
[13] A. Splendiani, L. Sun, Y. Zhang, T. Li, J. Kim, C.-Y. Chim, G. Galli, F. Wang, *Nano Lett.* **2010**, *10*, 1271.
[14] H. S. S. Ramakrishna Matte, A. Gomathi, A. K. Manna, D. J. Late, R. Datta, S. K. Pati, C. N. R. Rao, *Angew. Chem. Int. Ed.* **2010**, *49*, 4059.
[15] K.-K. Liu, W. Zhang, Y.-H. Lee, Y.-C. Lin, M.-T. Chang, C.-Y. Su, C.-S. Chang, H. Li, Y. Shi, H. Zhang, C.-S. Lai, L.-J. Li, *Nano Lett.* **2012**, *12*, 1538.
[16] Y.-H. Lee, X.-Q. Zhang, W. Zhang, M.-T. Chang, C.-T. Lin, K.-D. Chang, Y.-C. Yu, J. T.-W. Wang, C.-S. Chang, L.-J. Li, T.-W. Lin, *Adv. Mater.* **2012**, *24*, 2320.
[17] H. Pan, Y.-W. Zhang, *J. Mater. Chem.* **2012**, *22*, 7280.
[18] S. Wu, Z. Zeng, Q. He, Z. Wang, S. J. Wang, Y. Du, Z. Yin, X. Sun, W. Chen, H. Zhang, *Small* **2012**, *8*, 2264.
[19] P. Krüger, M. Petukhov, B. Domenichini, A. Berkó, S. Bourgeois, *J. Phys. Chem. C* **2012**, *116*, 10617.
[20] T. Cao, G. Wang, W. Han, H. Ye, C. Zhu, J. Shi, Q. Niu, P. Tan, E. Wang, B. Liu, J. Feng, *Nat. Commun.* **2012**, *3*, 887.
[21] A. Castellanos-Gomez, M. Barkelid, A. M. Goossens, V. E. Calado, H. S. J. van der Zant, G. A. Steele, *Nano Lett.* **2012**, *12*, 3187.
[22] H. S. Lee, S.-W. Min, Y.-G. Chang, M. K. Park, T. Nam, H. Kim, J. H. Kim, S. Ryu, S. Im, *Nano Lett.* **2012**.
[23] Y. Zhang, J. Ye, Y. Matsuhashi, Y. Iwasa, *Nano Lett.* **2012**, *12*, 1136.
[24] J. Brivio, D. T. L. Alexander, A. Kis, *Nano Lett.* **2011**, *11*, 5148.
[25] D. J. Late, B. Liu, H. S. S. R. Matte, V. P. Dravid, C. N. R. Rao, *ACS Nano* **2012**, *6*, 5635.
[26] K. F. Mak, K. He, J. Shan, T. F. Heinz, *Nat. Nanotechnol.* **2012**.

[27] Z. Zeng, T. Sun, J. Zhu, X. Huang, Z. Yin, G. Lu, Z. Fan, Q. Yan, H. H. Hng, H. Zhang, *Angew. Chem. Int. Ed.* **2012**, *51*, 9052.
[28] H. Li, G. Lu, Z. Yin, Q. He, H. Li, Q. Zhang, H. Zhang, *Small* **2012**, *8*, 682.
[29] Q. He, Z. Zeng, Z. Yin, H. Li, S. Wu, X. Huang, H. Zhang, *Small* **2012**, *8*, 2994.
[30] Q. H. Wang, K. Kalantar-Zadeh, A. Kis, J. N. Coleman, M. S. Strano, *Nat. Nanotechnol.* **2012**, *7*, 699.
[31] F. Xia, T. Mueller, Y.-m. Lin, A. Valdes-Garcia, P. Avouris, *Nat. Nanotechnol.* **2009**, *4*, 839.
[32] F. Xia, T. Mueller, R. Golizadeh-Mojarad, M. Freitag, Y.-m. Lin, J. Tsang, V. Perebeinos, P. Avouris, *Nano Lett.* **2009**, *9*, 1039.
[33] M. Y. Han, B. Özyilmaz, Y. Zhang, P. Kim, *Phys. Rev. Lett.* **2007**, *98*, 206805.
[34] X. Li, X. Wang, L. Zhang, S. Lee, H. Dai, *Science* **2008**, *319*, 1229.
[35] Y. Zhang, T.-T. Tang, C. Girit, Z. Hao, M. C. Martin, A. Zettl, M. F. Crommie, Y. R. Shen, F. Wang, *Nature* **2009**, *459*, 820.
[36] F. Xia, D. B. Farmer, Y.-m. Lin, P. Avouris, *Nano Lett.* **2010**, *10*, 715.
[37] F. Sols, F. Guinea, A. H. C. Neto, *Phys. Rev. Lett.* **2007**, *99*, 166803.
[38] L. Jiao, L. Zhang, X. Wang, G. Diankov, H. Dai, *Nature* **2009**, *458*, 877.
[39] A. O'Neill, U. Khan, J. N. Coleman, *Chem. Mater.* **2012**, *24*, 2414.
[40] S. Balendhran, J. Z. Ou, M. Bhaskaran, S. Sriram, S. Ippolito, Z. Vasic, E. Kats, S. Bhargava, S. Zhuiykov, K. Kalantar-zadeh, *Nanoscale* **2012**, *4*, 461.
[41] C. Lee, H. Yan, L. E. Brus, T. F. Heinz, J. Hone, S. Ryu, *ACS Nano* **2010**, *4*, 2695.
[42] H. Li, Q. Zhang, C. C. R. Yap, B. K. Tay, T. H. T. Edwin, A. Olivier, D. Baillargeat, *Adv. Funct. Mater.* **2012**, *22*, 1385.
[43] E. Bekyarova, M. Davis, T. Burch, M. E. Itkis, B. Zhao, S. Sunshine, R. C. Haddon, *J. Phys. Chem. B* **2004**, *108*, 19717.